Accepted Manuscript

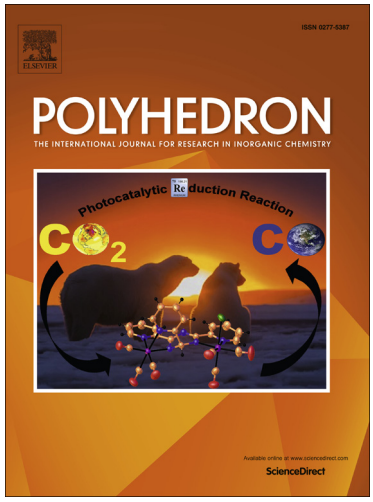

New Mixed-Ligand 8-Hydroxyquinolinato Iron(III) Complexes of Dimethylethylenediamine-based Aminophenol Ligands

Elham Safaei, Narges Naghdi, Andrzej Wojtczak, Zvonko Jagličić

PII: S0277-5387(16)00082-6
DOI: http://dx.doi.org/10.1016/j.poly.2016.01.049
Reference: POLY 11812

To appear in: *Polyhedron*

Received Date: 4 November 2015
Accepted Date: 29 January 2016

Please cite this article as: E. Safaei, N. Naghdi, A. Wojtczak, Z. Jagličić, New Mixed-Ligand 8-Hydroxyquinolinato Iron(III) Complexes of Dimethylethylenediamine-based Aminophenol Ligands, *Polyhedron* (2016), doi: http://dx.doi.org/10.1016/j.poly.2016.01.049

New Mixed-Ligand 8-Hydroxyquinolinato Iron(III) Complexes of Dimethylethylenediamine-based Aminophenol Ligands

Elham Safaei [a,b], Narges Naghdi [b], Andrzej Wojtczak[c], Zvonko Jagličić[d],

[a]Department of Chemistry, College of Sciences, Shiraz University, Shiraz, 71454, Iran
[b]Institute for Advanced Studies in Basic Sciences (IASBS), 45137-66731, Zanjan, Iran
[c]Nicolaus Copernicus University, Department of Chemistry, 87-100, Torun, Poland
[d]Institute of Mathematics, Physics and Mechanics & Faculty of Civil and Geodetic Engineering, University of Ljubljana, Jadranska 19. SI-1000, Ljubljana, Slovenia
Correspondence to: Elham Safaei

E-mail:e.safaei@shirazu.ac.ir

Four new mixed ligand iron(III) complexes of N,N'-dimethylethylenediamine based bis(phenol) di-amine (H_2L^{NER}) and 8-hydroxyquinoline (HQ) ligands have been synthesized and characterized by spectroscopic methods, X-ray diffraction, magnetic susceptibility measurements and cyclic voltammetry techniques. X-ray structure analysis revealed iron complexes with monoclinic or triclinic structures in which the H_2L^{NEX} and HQ ligands are coordinated to the Fe(III) center. The variable temperature magnetic susceptibility indicated a paramagnetic iron(III) center in the complexes. Electrochemical studies of the complexes with cyclic voltammetry showed cathodic peaks corresponding to an Fe^{III} to Fe^{II} reduction. An anodic peak was found that corresponded to phenolate ligand oxidation to phenoxyl radicals in the positive potential regions. To the best of our knowledge, synthesis reports on mixed-ligand 8-hydroxyquinolinato iron(III) complexes are very rare.

Keywords: Bis(phenol) di-amine; 8-hydroxyquinoline; Tripodal ligands, Enzyme models, Enzyme-substrate

Introduction

Tripodal ligands are tri- and tetradentate ligands which are popular in coordination chemistry and homogeneous catalysis research areas. As these ligands are polydentate, they have been used in the synthesis of metal complexes as model complexes for the active site of various enzymes. Many efforts have been devoted to the design and synthesis of new chelating ligands with the aim of enhancing their ability to form complexes with metal ions such as copper, iron and manganese that model the active site of the enzyme galactose oxidase, [1-5] various dioxygenases, lipoxygenases and phosphatases [6-11]. Lipoxygenases (Scheme 1) are a family of iron-containing enzymes that catalyze the dioxygenation of polyunsaturated fatty acids into hydroperoxides using molecular oxygen as an oxidant. These natural compounds play an important role in plants, animals and fungi physiology, including growth and development, resistance or response to pest or wounding [12]. The active site of the enzyme contains an iron atom which is bound by five ligands, three or four of which are histidine residues and one or two oxygen atoms of carboxylate groups [13-16]. The coordination number of the iron center is either five or six, with additional hydroxyl or water ligands for a hexacoordinate iron center.

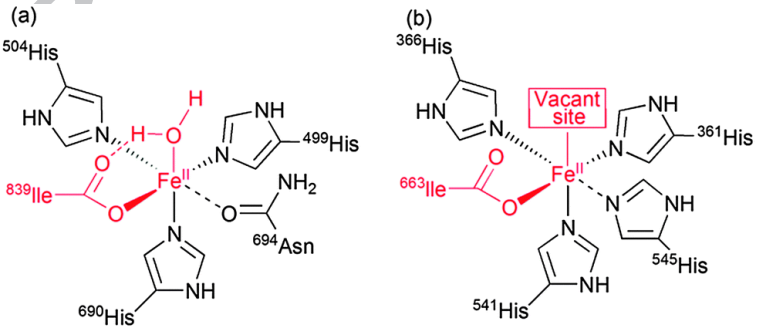

Scheme 1. The active site of lipoxygenase enzyme [17]

In soil bacteria, catechol dioxygenase enzymes catalyze the aerobic cleavage of catechol to aliphatic acids and other dihydroxy aromatics. The active site of these enzymes contains Fe(II) or Fe(III) ions (Scheme 2). Prior to catechol binding, the ferric or ferro ion is coordinated by four amino acid residues, i.e. histidine (His) and tyrosine (Tyr) or glutamic acid and a hydroxyl or H_2O molecule. Catecholate binding results in the displacement of non-amino acid ligands and the active-site geometry of the enzyme-catecholate complexes could be described as octahedral with mixed ligands [18,19].

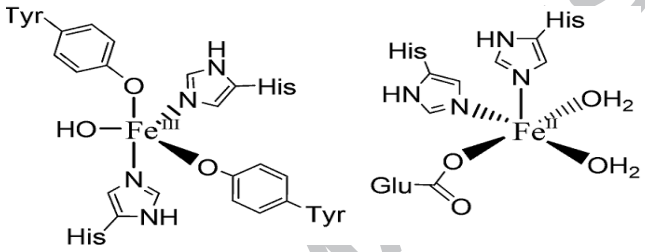

Scheme 2. The active site of dioxygenase enzymes [18]

Significant efforts have been made towards the synthesis of iron complexes using tripodal ligands with exclusively oxygen and nitrogen donor atoms [20-30] that mimic the architecture of enzyme active sites or mixed ligand complexes of enzyme-substrate adducts.

The main focus of this project was the synthesis, characterization and X-ray structures of a series of mixed ligand Fe(III) complexes of N,N'-dimethylethylenediamine based bis(phenol) di-amine (H_2L^{NER}) and 8-hydroxy quinolone (HQ) ligands (Scheme 3).

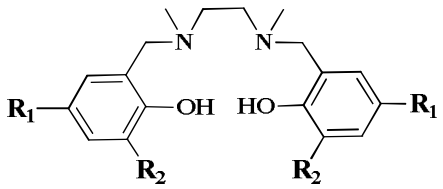

H_2L^{NER}	R_1	R_2
H_2L^{NEC}	Cl	Cl
H_2L^{NEB}	Br	Br
H_2L^{NEM}	Me	Me
H_2L^{NEOB}	OMe	^{t}Bu

Scheme 3. The structure of bis(phenol) di-amine, H_2L^{NER}

2. Experimental

2.1. Materials and physical measurements

Reagents or analytical grade materials were obtained from commercial suppliers and used without further purification, except those for electrochemical measurements. Fourier transform infrared spectroscopy on KBr pellets was performed on a FT-IR Bruker Vector 22 instrument. UV-Vis absorbance digitized spectra were collected using a CARY 100 spectrophotometer. Magnetic susceptibility was measured for powder samples of solid materials over the temperature range 2-300 K using a SQUID susceptometer (Quantum Design MPMS-XL-5) at a constant field of 1000 Oe.

Voltammetric measurements were made with a computer controlled electrochemical system (ECO Chemie, Utrecht, The Netherlands) equipped with a PGSTA 30 model and driven by GPES (ECO Chemie). A glassy carbon electrode with a surface area of 0.035 cm^2 was used as a working electrode and a platinum wire served as the counter electrode. The reference electrode was an Ag wire as a quasi-reference electrode. Ferrocene was added as an internal standard after completion of the experiment set-up, and potentials are referenced vs. the ferrocenium/ferrocene couple (Fc^+/Fc).

Crystals for the X-ray diffraction experiment were obtained from an EtOH-CH_2Cl_2 solution. X-ray diffraction data were collected with an Oxford Sapphire CCD diffractometer using

MoKα radiation, λ =0.71073 Å, at 293(2) K, by the ω-2θ method. For $FeQL^{NEOB}$, the space group was triclinic P-1. For the other complexes, space groups were assigned as monoclinic $P2_1/c$, based on systematic absences. The structures were solved by direct methods and refined with the full-matrix least-squares method on F^2 with the use of the SHELX97 [31] program package. Analytical absorption corrections were applied (Table 1) (RED171 package of programs [32] Oxford Diffraction, 2000). No extinction correction was applied. For all reported structures, hydrogen atoms were located from the electron density maps and their positions were constrained in the refinement.

2.2. Preparation

All the ligands were synthesized based on literature reports [33].

2.2.1. Synthesis of the $FeQL^{NER}$ complexes

To a stirred mixture of H_2L^{NER} (1.00 mmol), 8-hydroxyquinoline (0.14 g, 1.00 mmol) and triethylamine (0.30 g, 3.00 mmol) in ethanol (50 ml), $FeCl_3$ (0.16 g, 1.00 mmol) was added under continuous stirring. The reaction mixture was then refluxed for 1 h. The solvent was evaporated and a red brown powder was obtained. Red brown colored crystals suitable for X-ray diffraction were obtained by slow evaporation of a dichloromethane and ethanol solution of the powder.

2.2.1.1. Synthesis of $FeQL^{NEM}$

Yield: 63%. Anal. calcd. for $C_{31}H_{36}FeN_3O_3$ (554.48 g/mol): Fe, 10.02; C, 65.00; H, 6.38; N, 7.10%. Found: Fe, 10.70; C, 65.25; H, 6.54; N, 7.58%. IR (KBr, cm^{-1}): 3779, 3450, 2959, 2907, 2283, 1573, 1466, 1376, 1317, 1273, 1218, 1111, 1026, 973, 875, 831, 782, 742, 611, 516.

2.2.1.2. Synthesis of $FeQL^{NEB}$

Yield: 55%. Anal. calcd. for $C_{27}H_{24}Br_4FeN_3O_3$ (813.98 g/mol): Fe, 6.28; C, 39.10; H, 2.49; N, 4.86%. Found: Fe, 6.31; C, 39.24; H, 2.97; N, 5.06%. IR (KBr, cm^{-1}): 3804, 3435, 2918,

1633, 1574, 1451, 1376, 1317, 1271, 1221, 1153, 1106, 1057, 861, 817, 745, 709, 562, 511, 465.

2.2.1.3. Synthesis of $FeQL^{NEOB}$

Yield: 58%. Anal. calcd. for $C_{37}H_{48}FeN_3O_5$ (670.63 g/mol): Fe ,8.02; C, 64.20; H, 7.20; N, 5.80%. Found: Fe, 8.1; C, 65.26; H, 7.21; N, 6.01%. IR (KBr, cm^{-1}): 3439, 2944, 2751, 2678, 2492, 1606, 1460, 1381, 1317, 1268, 1204, 1140, 1104, 1052, 858, 820, 791, 740, 519, 473.

2.2.1.4. Synthesis of $FeQL^{NEC}$

Yield: 60%. Anal. calcd. for $C_{27}H_{26}Cl_4FeN_3O_4$ (654.16 g/mol): Fe ,8.02; C, 49.25; H, 3.20; N, 6.40%. Found: Fe, 8.11; C, 50.08; H, 3.30; N, 6.48%. IR (KBr, cm^{-1}): 3444, 2914, 1580, 1455, 1374, 1317, 1219, 1170, 1055, 865, 828, 751, 571, 515, 459.

3. Results and discussion

3.1. Ligand and complex synthesis and characterization

The strategy applied to prepare the tripodal ligands based on a tertiary amine was the one step Mannich reaction; N,N'-dimethylethylenediamine was treated with phenol (with different substituents in the 2 and 4 positions) and paraformaldehyde under solvent free conditions. Both the ligand and the used reaction method have been reported in literature [33,34]. An overview of the synthesized $FeQL^{NER}$ complexes is given in Scheme 4. The obtained complexes have the general formula $FeQL^{NER}$, in which L^{NER} is one of the dianionic ligands H_2L^{NEX} and "Q" is 8-oxyquinoline (quin). The general method used to prepare these complexes was to react an iron(III) chloride complex with the tripodal ligand and 8-oxyquinoline in ethanol, with the addition of 2 equivalents of triethylamine. The complexes were obtained with high purity and quite a high overall yield.

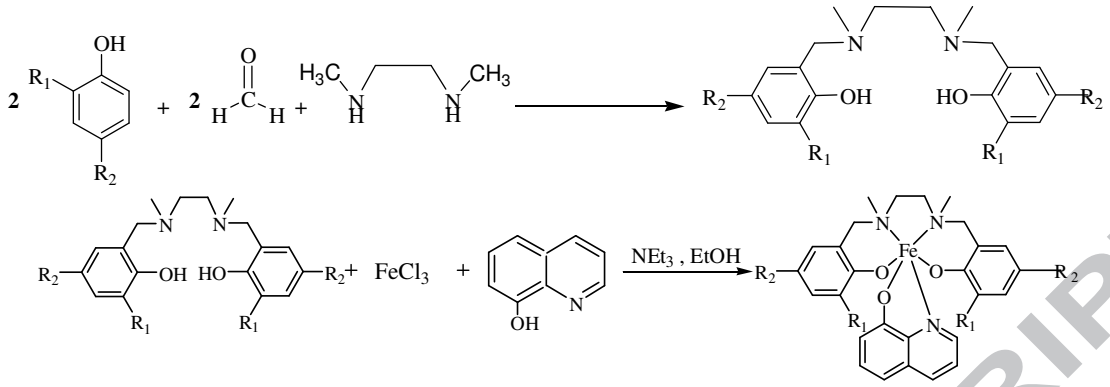

Scheme 4. The reaction pathway for the synthesis of the complexes

3.1.1. X-ray crystal structures of the FeQL^{NER} complexes

The diffraction experiments and the structure refinements for the complexes are summarized in Table 1. Selected bond lengths and angles are given in Tables 2 and 3.

Table 1.

Table 2.

Table 3.

The FeQL^{NEB}, FeQL^{NEC} and FeQL^{NEM} complexes crystallize in the monoclinic space group $P2_1/c$, while FeQL^{NEOB} crystallizes in the triclinic space group P-1. For FeQL^{NEB}, FeQL^{NEM} and FeQL^{NEOB}, the asymmetric part of the structure consists of a single complex molecule, while in FeQL^{NEC} it consists of two complex molecules and two water molecules (Figs. 1-4). For all the complexes, the FeN_3O_3 coordination sphere has an octahedral geometry. The Q ligand is bidentately coordinated to the Fe(III) ion via the phenolate O3 (O5 for FeQL^{NEOB}) and pyridine N3 atoms. L^{NEX} acts as a tetradentate ligand with the phenolate O1 and O2 atoms occupying cis positions. In all the reported complexes, one phenolate O atom is positioned trans to the hydroxyquinoline O3 atom, and one N atom of the central ethylenediamine bridge is positioned trans to the hydroxyquinoline N3 atom. The S,S-N1,N2 configuration is found for the FeQL^{NEB}, FeQL^{NEM} and FeQL^{NEOB} molecules in the asymmetric unit, although the opposite R,R configuration occurs in the other molecule due to

the centrosymmetric space group $P2_1/c$. In contrast, for $FeQL^{NEC}$ there is a difference in the chirality of the N centers between two complex molecules constituting the asymmetric unit of the structure. For molecule 1, the configuration is S,S-N1,N2, while in molecule 2, the R,R-N31,N32 configuration is found. Analysis reveals, however, that there is no center of symmetry or symmetry plane relating these molecules. Interestingly, only a non-crystallographic two-fold axis can be found with the rotation of [1.000 -0.216 0.482] -175.22^o [35], that might relate molecule 1 to molecule 2, but with the chirality of the latter inverted relative to that observed in the real structure.

Fig. 1- Fig. 4

Similar to other complexes containing L^{NEB} or analogous ligands [33,34,36,37], in the structures reported here the Fe-O1 and Fe-O2 bonds involving the L^{NEX} phenolate atoms are shortest within the coordination sphere, ranging from 1.8777(15) to 1.926(3) Å. These values are significantly shorter than those of Fe1-O1 1.937(9) and Fe1-O2 1.955(8) Å reported for the FeL^{NEB}(TBC) complex [33], where TBC is tetrabromocatecholate. The Fe-O3 bonds formed by the phenolate group of Q are significantly longer, with distances ranging from 1.978(2) to 2.009(2) Å. Also in all the complexes reported here, the Fe-N2 and Fe-N1 bonds formed by the ethylenediamine moiety [2.173(3) to 2.323(3) Å] are significantly longer than the Fe-N3 bonds formed by the N atom of the hydroxyquinoline ligand [2.132(3) to 2.1651(19) Å] (Table 2). Significant bulk is introduced in the vicinity of the central ion due to the bidentate coordination of the rigid Q ligand. In particular, the direct coordination of the ring system via the N3 atom results in deformation of the Fe coordination sphere. As a result, the longest bond within the coordination sphere of all the complexes is formed by the N atom of the ethylenediamine bridge, which is positioned cis to both the N and O atoms of the Q ligand.

The valence geometry of the 8-hydroxyquinoline ligand is typical. The valence geometry of the L^{NER} ligand is typical for such systems, as found in complexes reported before [33,34,36,37]. In $FeQL^{NEB}$, the C-Br distances range from C2-Br1 of 1.882(9) to C15-Br4 of 1.925(10) Å, almost identical to those reported for FeL^{NEB}(TBC) [36]. For $FeQL^{NEC}$, the C-Cl distances range from C2-Cl1 of 1.715(4) to C34-Cl32 of 1.752(4) Å, which and are similar to those reported for FeL^{NEC}(TBC) [33].

Similar to the FeL^{NEX} or μ-oxo-FeL^{NEX} complexes reported before, in all the $FeQL^{NER}$ complexes reported here, the conformation of the ethylenediamine bridge is synclinal. In $FeQL^{NEB}$ and $FeQL^{NEOB}$, the N1-C8-C9-N2 torsion angle is 54.8(9) and 58.6(3)°, respectively, and these values are similar to those found in the FeL^{NEB}(TBC) [33] and FeL^{NEOB} complexes [33]. In $FeQL^{NEM}$, this torsion angle (61.2(4)°) is larger than those reported before for FeL^{NEM} [34] or μ-oxo-FeL^{NEM} [36]. In $FeQL^{NEC}$, the conformation of the ethylenediamine moiety is also synclinal, in molecule 1 the N1-C8-C9-N2 torsion angle being 55.4(4)° and in molecule 2 the N31-C38-C39-N32 torsion angle being -57.6(5)°; the absolute values are almost identical to that reported for FeL^{NEC}-TBC [36].

With such a conformation of the ethylenediamine bridge, the dihedral angle between the two phenolic rings in $FeQL^{NEB}$ is 80.5(4)°, smaller than that of 85.9° found for FeL^{NEB}(TBC), and the angles between the N3--C26 best plane of the Q ligand and C1--C6 and C11--C16 phenolic planes are 71.6(3) and 68.0(4)°, respectively. For $FeQL^{NEOB}$, the dihedral angle between the two phenolic rings of L^{NEOB} is 75.16(13)°, a value significantly larger than that of 69.95° found in FeL^{NEOB} [33], and the angles between the N3--C26 Q best plane and C1--C6 and C11--C16 phenolic planes are 89.79(10) and 88.06(13)°, almost 20° larger than those found in $FeQL^{NEB}$. In the $FeQL^{NEM}$ structure, the dihedral angle between the two phenolic rings of L^{NEOB} is 89.2(2)°, the largest value found for the series of investigated complexes. It is, however, similar to that of 88.98° reported for μ-ox-FeL^{NEM}

[36]. On the other hand, the analogous dihedral angle in FeL^{NEM} is only 74.0° [34]. The angles between the N3--C26 best plane of the Q ligand and the C1--C6 and C11--C16 phenolic planes are 83.62(17) and 66.57(19)°, the former being slightly smaller than those found in $FeQL^{NEOB}$, while the latter is similar to those found in $FeQL^{NEB}$.

In $FeQL^{NEC}$, the dihedral angle between the two phenolic rings of L^{NECl} is 87.40(18)° in molecule 1 and 82.24(18)° in molecule 2, the values being between that of 80.5(4)° found for the analogous complex of L^{NEB} and 87.5° found for FeL^{NEC}(TBC) [33], but being significantly larger than that found for FeL^{NEC} [34]. The Q ligand is almost perpendicular to the phenolic rings of L^{NEC}, with dihedral angles between the best plane of the Q ligand and the phenolic C1--C6 and C11--C16 rings in molecule 1 being 83.49(16) and 86.72(15)°, and the corresponding angles being 83.66(15) and 83.26(15)° in molecule 2. These values are much larger than those found for $FeQL^{NEB}$.

Four chelate rings are formed in the $FeQL^{NER}$ complex molecules and the ring puckering was analyzed according to Cremer and Pople [38]. In $FeQL^{NEB}$, the Fe1-O3-C26-C27-N3 ring is flat, Fe1-N1-C8-C9-N2 is an envelope on C9, ring Fe1-O1-C1-C6-C7-N1 has a boat conformation, while Fe1-O2-C16-C11-C10-N2 is a screw-boat. For $FeQL^{NEOB}$, the conformation of the chelate ring Fe1-O5-C36-C37-N3 is twisted on Fe1-O5 and that of Fe1-N1-C8-C9-N2 is twisted on C8-C9, Fe1-O1-C1-C6-C7-N1 and Fe1-O2-C16-C11-C10-N2 are a half-chair and an envelope, respectively. In $FeQL^{NEM}$, the conformation of the chelate ring Fe1-O5-C36-C37-N3 is an envelope on Fe1, Fe1-N1-C8-C9-N2 is an envelope on C9, the conformations of both Fe1-O1-C1-C6-C7-N1 and Fe1-O2-C16-C11-C10-N2 are a screw-boat. In $FeQL^{NEC}$, the conformations of the chelate rings in molecule 1 are: Fe1-O3-C26-C27-N3 twisted on N3-Fe1, Fe1-N1-C8-C9-N2 an envelope on C8, Fe1-O1-C1-C6-C7-N1 half-chair, Fe1-O2-C16-C11-C10-N2 a screw-boat. For molecule 2: Fe2-O33-C56-C57-N33

is flat, Fe2-N31-C38-C39-N32 an envelope on C39, Fe2-O31-C31-C36-C37-N31 a screw-boat and Fe2-O32-C46-C41-C40-N32 an envelope.

3.1.2. Electronic absorption spectra of the complexes

The electronic absorption spectra of the complexes were obtained in the range 200-800 nm (Figure 5, Table 4) and reflect the electronic properties of the iron(III) complexes. The visible spectra of the complexes are dominated by two important charge transfer (CT) bands. All the complexes exhibit an intense absorption band (Figure 5, Table 4) at 288-310 nm (10^4-10^5 M^{-1} cm^{-1}) with a shoulder caused by $\pi \rightarrow \pi^*$ CT transitions involving the phenolate and 8-hydroxyquinoline units. The remaining lower energy bands (480-550 nm (10^4 $M^{-1}cm^{-1}$)) are relatively less intense, which indicates that they are associated with the 8-hydroxyquinoline-to-metal and phenolate-to-metal LMCT transitions [38]. A red shift of the position of the LMCT bands of complexes to higher wavelengths can be observed when the substituents on the phenolate groups are electron-donating, which would raise the energy of the frontier orbitals of the ligand and thus minimize the ligand-to-iron gap.

Figure 5

Table 4

3.1.3. Magnetic susceptibility measurements

In the magnetic susceptibility diagrams, the susceptibilities of the investigated samples increase with decreasing temperature (Figure 6). The analysis of the susceptibility $\chi(T)$ was performed by applying the Curie-Weiss law, $\chi = \frac{C}{(T-\theta)}$, for T > 50 K, which gives us information on the magnitude of magnetic moments $\mu_{eff} = \sqrt{8C}$ through the Curie-Weiss constant *C*. Above T ≈ 15 K, the effective magnetic moments (μ_{eff}) of the complexes (Figure 7). are essentially temperature-independent and have μ_{eff} values between 5.2-6.3 μ_B, which is

in good agreement with the expected value (5.92 μ_B) for an isolated S = 5/2 Fe(III) ion [39-42]. The obtained fitting parameters C, θ and μ_{eff} are listed in Table 5.

Small non-zero values of the Curie-Weiss temperatures θ can be regarded only as additional fitting parameters that slightly improve the fit. No evidence of any antiferromagnetic or ferromagnetic interactions between the iron magnetic centers can be deduced from the measured data. A minute temperature dependence of the effective magnetic moment at the lowest temperature may be attributed to zero-field splitting.

Figure 6

Figure 7

Table 5

3.1.4. Electrochemistry

The cyclic voltammograms (CV) of the complexes have been recorded in CH_2Cl_2 solutions containing 0.1 M $[(n\text{Bu})_4\text{N}]ClO_4$ as the supporting electrolyte. The $FeQL^{NER}$ irreversible metal-centered voltammograms have been observed in the negative potential range, which corresponds to the Fe^{III}/Fe^{II} reduction of the iron complexes. The voltammograms for all the complexes are typical of mononuclear complexes, since they show only one redox metal-centered process in the range -0.79 to -1.2 V. This observation is in agreement with the X-ray analysis results. A typical cyclic voltammogram (CV) for the reduction process of $FeQL^{NEOB}$ is presented in Fig. 8. Selected results for E_{peak} for the complexes are collected in Table 6. The E_R value for the $FeQL^{NER}$ complexes decreases in the order $FeQL^{NEOB}$ > $FeQL^{NEM}$ > $FeQL^{NEB}$ > $FeQL^{NEC}$, which means that the two last complexes present less negative redox potentials than the $FeQL^{NEOB}$ and $FeQL^{NEM}$ complexes, attributed to the most acidic iron(III) centers in these complexes. This observation may be ascribed to the presence of the chloro and bromo ligands placed on the phenolate groups, which decreases the electron density and consequently increases the Lewis acidity of the iron center. $FeQL^{NEOB}$ presents the least acid

iron(III) center, related to electron donation of the alkoxide group in the ligand structure. In addition, nearly similar redox potentials of the iron centers in all the complexes confirms the similarity of the coordination environment of the iron centers in all the complexes (N_2O_2). Our results reveal oxidation peak(s) for the $FeQL^{NER}$ complexes with a similar small difference in their redox potentials in the positive region (Figure 9). This small difference also supports that the coordination environment around the metal center in all the complexes should be similar, as mentioned above. These redox processes might be attributed to the presence of Fe(III)-phenoxyl radical species [41-43] during the cyclic voltammetry experiments, a kind of ligand centered redox process in which the phenolate group yields a phenoxyl radical, though there is no direct evidence available for this yet. Similar observations have been described previously in other compounds containing *tert*-butylphenol ligands, being ascribed as the oxidation of this unit and the generation of the phenoxyl radical [44-46]. $FeQL^{NEOB}$ showed two quasi-reversible oxidative process, centered on the ligand, indicating that the first oxidation peak must be due to mono radical cation formation on one phenolate ring $[Fe\text{-}OPh^{\bullet}]^{+}$ and the second to either dication formation (this seems unlikely) or to the formation of a second radical cation on the other phenolate ring unit $[Fe\text{-}OPh^{\bullet\bullet}]^{+}$. The second oxidation peak is observed at higher potentials, which means that the second oxidation is harder relative to the oxidation of the radical cation complex. On the other hand, the other complexes show just one irreversible oxidative peak. Wieghardt's group have proposed that the lack of reversibility of these processes is attributed to a competitive chemical reaction (polymerization of phenoxyl radicals) which can be induced by the electrochemical process, resulting in the extinction of the radical species [47]. If we assume that in $FeQL^{NEOB}$, the first and second oxidation peaks are related to the formation of $[Fe\text{-}OPh^{\bullet}]^{+}$ $[Fe\text{-}OPh^{\bullet\bullet}]^{+}$ species while in other complexes there is just the production of $[Fe\text{-}OPh^{\bullet}]^{+}$ species, we can conclude that the $FeQL^{NEOB}$ phenoxyl radicals are much more stable

than the corresponding ones of the three other complexes. It considers that the tert-butyl groups placed on the phenolate rings prevent unwanted chemical reactions of the phenoxyl radicals, such as polymerization and C-C coupling, due to the high steric effect and inhibition of the sterically shielded phenoxyl radicals lying too close together. On comparison of the oxidation potentials of the complexes (Table 6), a red shift in the anodic oxidation peaks has been observed suggesting that the anodic processes are sensitive to the involved change in the electron accepting nature of the substituents on the phenolate moieties of the ligands. On the other hand, the oxidation potentials of the $FeQL^{NEC}$ and $FeQL^{NEB}$ complexes, with electron accepting ligands such as Cl, are more positive than $FeQL^{NEM}$ and $FeQL^{NEOB}$ (with electron donating methyl and methoxy groups) due to the harder oxidation of the phenolate ligands to the corresponding phenoxyl radical cations. These observations may be explained by the fact that the two last complexes represent the most acidic iron centers and that, due to this, the electron density is preferentially localized on the aromatic rings, which makes it easier to carry out their oxidation. Interestingly, $FeQL^{NEOB}$ shows the lowest 1st oxidation potential compared to the other complexess, so the 2nd oxidation process of $FeQL^{NEOB}$ related to the formation of a radical from a radical cation appears to align very well with the oxidation peak potential of the other three compounds with the production of a radial from a neutral compound. Such steric and electronic effects on the easy production and stability of radicals in the metalloradical world has been consider by nature for metalloenzymes [18].

Figure 8

Figure 9

Table 6

4. Conclusions

A series of new mixed ligand iron(III) complexes of N,N'-dimethylethylenediamine based bis(phenol) di-amine (H_2L^{NER}) and 8-hydroxyquinolone(HQ) ligands have been synthesized

and characterized. The complexes $FeQL^{NEB}$, $FeQL^{NEC}$, $FeQL^{NEM}$ and $FeQL^{NEOB}$ have been structurally characterized by single crystal X-ray diffraction. X-ray structure analysis has revealed that all the complexes are six coordinate and Fe(III) centers are surrounded by three phenolic oxygen atoms, comprising two oxygen atoms of H_2L^{NER} and another one from the HQ ligand, and three nitrogen atoms from both H_2L^{NER} and HQ ligands. Employing various ligands with electron-withdrawing or electron donating substituents on the phenolate arms, we have obtained different complexes, combinations with interesting variations in properties, which are useful in the study of a structure-activity relationship. The large influence of the ligand sets and the electron density of the metal centre on both the position of the CT transitions in the UV-vis spectra and the peak potentials in the CV measurements suggest that both redox and charge transfer processes are sensitive to the electron accepting properties of the substituents on the phenolate moieties of the ligands. The magnetic moment measurements confirm monomer complexes with paramagnetic Fe(III) centres.

Appendix A.

The crystallographic data have been deposited with the Cambridge Crystallographic Data Centre, with CCDC numbers: 1415983, 1415984, 1415985 and 1415986 for $FeQL^{NEB}$, $FeQL^{NEC}$, $FeQL^{NEM}$ and $FeQL^{NEOB}$, respectively. These data can be obtained free of charge via http://www.ccdc.cam.ac.uk/conts/retrieving.html or from the Cambridge Crystallographic Data Centre, 12 Union Road, Cambridge CB2 1EZ, UK; fax: (+44) 1223-336-033; or e-mail: deposit@ccdc.cam.ac.uk.

Acknowledgments

The authors are grateful to the Institute for Advanced Studies in Basic Sciences (IASBS), Nicolaus Copernicus, Ljubljana Universities for their valuable help. E. Safaei gratefully

acknowledges the support by the Institute for Advanced Studies in Basic Sciences (IASBS) Research Council under Grant No. G2015IASBS127.

References

[1] L. Jr. Que, W. B. Tolman, Nature 455 (2008) 333-340.

[2] L. Xie, PNAS 98 (2001) 12863-12865.

[3] N. Ito, S. E. V. Phillips, C. Stevens, Z. B. Ogel, M. J. McPherson, J. N. Keen, K. D. S. Yadav, P. F. Knowles, Nature, 350 (1991) 87-90.

[4] F. Michel, F. Thomas, S. Hamman, C. Philouze, E. Saint-Aman, J. L. Pierre, Eur. J. Inorg. Chem. (2006) 3684-3696.

[5] [M.M. Whittaker, J.W. Whittaker, J. Biol. Chem. 265 (1990) 9610-9613.

[6] Y. Zang, J. Kim, Y. Dong, E.C. Wilkinson, E.H. Appelman, L. Que, J. Am. Chem. Soc. 119 (1997) 4197-4205.

[7] Y.-M. Chiou, L. Que, Inorg. Chem. 34 (1995) 3577-3578.

[8] M. Velusamy, R. Mayilmurugan, M. Palaniandavar, Inorg. Chem. 43 (2004) 6284-6293.

[9] M. Costas, M.P. Mehn, M.P. Jensen, L. Que, Chem. Rev. 104 (2004) 939-986.

[10] T. Funabiki, D. Sugio, N. Inui, M. Maeda, Y. Hitomi, Chem. Commun. (2002) 412-413.

[11] M. Velusamy, M. Palaniandavar, R.S. Gopalan, G.U. Kulkarni, Inorg. Chem. 42 (2003) 8283-8293.

[12] J. Choi, JK. Chon, S. Kim, W. Shin, Proteins 70 (2008)1023-32.

[13] BA. Vick, DC. Zimmerman. "Oxidative systems for the modification of fatty acids" (1987) 9. pp. 53–90.

[14] P. Needleman, J. Turk, BA. Jakschik, AR. Morrison, JB. Lefkowith "Arachidonic acid metabolism". Annu. Rev. Biochem. 55 (1986) 69-102.

[15] K. Tanaka, H. Ohta, YL. Peng, Y. Shirano, T. Hibino, D. Shibata, J. Biol. Chem. 269 (1994) 3755-3761.

[16] S. Xu, T. C. Mueser, L. J. Marnett, M. O. Funk Jr., Structure 20 (2012) 1490-1497.

[17] Z. Chen, G. Yin, Chem. Soc. Rev. 44 (2015) 1083-1100.

[18] T. E. Elgren, A. M. Orville, K. A. Kelly, J. D. Lipscomb, D. H. Ohlendorf, L. Que Jr., Biochemistry 36 (1997) 11504 -11513.

[19] D. H. Ohlendorf, J. D. Lipscomb, P. C. Weber, Nature 336 (1988) 403-405.

[20] M. Velusamy, M. Palaniandavar, R.S. Gopalan, G.U. Kulkarni, Inorg. Chem. 42 (2003) 8283-8293.

[21] S.P. Yan, X.Y. Pan, L.F. Taylor, J.H. Zhang, C.J. Oconnor, D. Britton, O.P. Anderson, L. Que, Inorg. Chim. Acta 243 (1996) 1-8.

[22] R. van Gorkum, E. Bouwman, Coord. Chem. Rev. 249 (2005) 1709-1728.

[23] J. Mallegol, A. M. Barry, E. Ciampi, P. M. Glover, P. J. McDonald, J. L. Keddie, M. Wallin, J. Coat. Technol. 74 (2002)113-124.

[24] H. W. Gardner, Current Protocols in Food Analytical Chemistry, (2001) 4.2.1.

[25] J. Mallegol, J. Lemaire, J. L. Gardette, Prog. Org. Coat. 39 (2000) 107-113.

[26] S. T. Warzeska, M. Zonneveld, R. van Gorkum, W. J. Muizebelt, E. Bouwman, J. Reedijk, Prog. Org. Coat. 44 (2002), 243-248.

[27] Z. O. Oyman, W. Ming, R. van der Linde, R. van Gorkum, E. Bouwman, Polymer 46 (2005) 10531-10537.

[28] R. van Gorkum, E. Bouwman, J. Reedijk, Inorg. Chem. 43 (2004) 2456-2458.

[29] R. van Gorkum, E. Bouwman, J. Reedijk, patent EP1382648, 2004.

[30] R. van Gorkum, F. Buda, H. Kooijman, A. L. Spek, E. Bouwman, J. Reedijk, Eur. J. Inorg. Chem. (2005) 2255-2261.

[31] G. M. Sheldrick, Acta Cryst. A 64 (2008) 112-122.

[32] CrysAlis CCD171 and RED171 package of programs, Oxford Diffraction, 2000.

[33] T. Karimpour, E. Safaei, A. Wojtczak, Z. Jaglic˘ic´, A. Kozakiewicz, Inorg. Chim. Acta 395 (2013) 124-134.

[34] S. Heidari, E. Safaei, A. Wojtczak, P. Cotic˘, A. Kozakiewicz, Polyhedron 55 (2013) 109-116.

[35] A.L. Mackay, Acta Cryst. (1984), A40, 165-166.

[36] T. Karimpour, E. Safaei, A. Wojtczak, Z. Jagličić, Inorg. Chim. Acta 405 (2013) 309-317.

[37] T. Karimpour, E. Safaei, A. Wojtczak, P. Cotic, J. Mol. Struct. 1038 (2013) 230-234.

[38] D. Cremer, J.A. Pople, J. Am. Chem. Soc. 97 (1975) 1354-1358

[39] M. Velusamy, M. Palaniandavar, R.S. Gopalan, G.U. Kulkarni, Inorg. Chem. 42 (2003) 8283-8293.

[40] Kahn, Molecular Magnetism, VCH Publishers, New York, 1993, pp. 86-90.

[41] N.W.Ashcroft, N.D. Mermin, Solid State Physics, Saunders College Publishing, New York, 1976, pp. 653-657.

[42] P. Basu, A. Chakravorty, J. Chem. Soc., Chem. Commun. (1992) 809-810.

[43] P. Basu, A. Chakravorty, Inorg. Chem. 31 (1992) 4980-4986.

[44] E. Safaei, T. Weyhermuller, E. Bothe, K. Wieghardt, P. Chaudhuri, Eur. J. Inorg. Chem. 16 (2007) 2334-2344.

[45] J. B. H. Strautmann, S. D. George, E. Bothe, E. Bill, T. Weyhermüller, A. Stammler, H. Bögge, T. Glaser, Inorg. Chem. (2008) 47, 6804-6824.

[46] P. Chaudhuri, K. Wieghardt, Prog. Inorg. Chem. (2001) 50, 151-216.

[47] S. Kimura, E. Bill, E. Bothe, T. Weyhermüller, K. Wieghardt, J. Am. Chem. Soc. (2001) 123, 6025-6039.

Table 1. Crystal data and structure refinement for $FeQL^{NEB}$, $FeQL^{NEC}$, $FeQL^{NEM}$ and $FeQL^{NEOB}$

	$FeQL^{NEB}$	**$FeQL^{NEOB}$**	**$FeQL^{NEM}$**	**$FeQL^{NEC}$**
Empirical formula	$C_{27}H_{24}Br_4FeN_3O_3$	$C_{37}H_{48}FeN_3O_5$	$C_{31}H_{36}FeN_3O_3$	$C_{54}H_{52}Cl_8Fe_2N_6O_8$
Formula weight	813.98	670.63	554.48	1308.32
Temperature; K	293(2)	293(2)	293(2)	293(2)
Wavelength; Å	0.71073	0.71073	0.71073	0.71073
Crystal system, space group	Monoclinic, $P2_1/c$	Triclinic, P-1	Monoclinic, $P2_1/c$	Monoclinic, $P2_1/c$
Unit cell dimensions;				
a, Å	11.0934(6)	11.2421(3)	16.9388(11)	12.2402(2)
b, Å	9.2948(6)	12.2205(4)	8.4293(4)	21.5512(3)
c, Å	28.0609(17)	15.1712(5)	21.4119(13)	22.7938(4)
α, °		75.212(3)		
β, °	96.683(5	74.490(3)	113.255(8)	102.5225(16)
γ, °		65.101(3)		
Volume; $Å^3$	2873.7(3)	1797.26(10)	2808.9(3)	5869.77(17)
Z, Calculated density; Mg/m^3	4, 1.881	2, 1.239	4, 1.311	4, 1.480
Absorption coefficient; mm^{-1}	6.121	0.464	0.573	0.916
F(000)	1588	714	1172	2680
Crystal size; mm	0.50 x 0.45 x 0.31	0.80 x 0.37 x 0.16	0.47 x 0.20 x 0.04	0.41 x 0.27 x 0.21
Theta range for data collection; °	2.31 to 26.00	2.15 to 26.00	2.07 to 28.17	2.21 to 28.16
Limiting indices	-13<=h<=12, -11<=k<=6, -32<=l<=34	-13<=h<=9, -14<=k<=15, -18<=l<=18	-20<=h<=21, -10<=k<=11, -28<=l<=26	-15<=h<=16, -28<=k<=26, -29<=l<=26
Reflections collected / unique	16206 / 5644 [R(int) = 0.0589]	11272 / 7042 [R(int) = 0.0344]	20677 / 6204 [R(int) = 0.0866]	35538 / 12823 [R(int) = 0.0291]
Completeness to theta	26.00 99.9 %	26.00 99.7 %	26.00 100.0 %	26.00 99.8 %
Absorption correction	Analytical	Analytical	Analytical	Analytical
Max. and min. transmission	0.2514 and 0.1493	0.9291 and 0.7075	0.9802 and 0.7740	0.8306 and 0.7070
Refinement method	Full-matrix least-squares on F^2	Full-matrix least-squares on F^2	Full-matrix least-squares on F^2	Full-matrix least-squares on F^2
Data / restraints / parameters	5644 / 0 / 343	7042 / 0 / 415	6204 / 0 / 343	12823 / 0 / 704
Goodness-of-fit on F^2	1.029	1.093	0.855	0.984
Final R indices [I>2sigma(I)]	R1 = 0.0678, wR2 = 0.1616	R1 = 0.0458, wR2 = 0.1260	R1 = 0.0586, wR2 = 0.1237	R1 = 0.0532, wR2 = 0.1651
R indices (all data)	R1 = 0.1372, wR2 = 0.1884	R1 = 0.0576, wR2 = 0.1340	R1 = 0.1441, wR2 = 0.1429	R1 = 0.0848, wR2 = 0.1772
Largest diff. peak and hole; $e.A^{-3}$	2.270 and -1.099	0.535 and -0.324	0.560 and -0.501	1.307 and -0.449

Table 2. Selected bond lengths [Å] and angles [deg] for $FeQL^{NEB}$, $FeQL^{NEOB}$, $FeQL^{NEM}$

$FeQL^{NEB}$		$FeQL^{NEOB}$		FeL^{NEM}	
Bond lengths/ Å					
Fe1-O1	1.918(5)	Fe1-O1	1.9036(15)	Fe1-O1	1.888(3)
Fe1-O2	1.891(6)	Fe1-O2	1.8777(15)	Fe1-O2	1.889(2)
Fe1-O3	1.984(5)	Fe1-O5	2.0077(15)	Fe1-O3	2.009(2)
Fe1-N3	2.159(7)	Fe1-N3	2.1651(19)	Fe1-N3	2.142(3)
Fe1-N2	2.194(6)	Fe1-N2	2.2084(17)	Fe1-N2	2.187(3)
Fe1-N1	2.323(7)	Fe1-N1	2.3066(19)	Fe1-N1	2.323(3)
Bond angles/°					
O2-Fe1-O1	95.5(3)	O2-Fe1-O1	96.26(7)	O1-Fe1-O2	94.20(11)
O2-Fe1-O3	96.1(3)	O2-Fe1-O5	93.66(7)	O1-Fe1-O3	169.05(10)
O1-Fe1-O3	162.6(2)	O1-Fe1-O5	164.93(7)	O2-Fe1-O3	95.28(11)
O2-Fe1-N3	93.0(3)	O2-Fe1-N3	101.34(7)	O1-Fe1-N3	94.99(12)
O1-Fe1-N3	88.2(2)	O1-Fe1-N3	89.10(7)	O2-Fe1-N3	97.91(10)
O3-Fe1-N3	78.4(2)	O5-Fe1-N3	77.83(7)	C1-O1-Fe1	138.1(2)
O2-Fe1-N2	87.4(2)	O2-Fe1-N2	86.27(6)	C8-N1-Fe1	105.2(2)
C26-O3-Fe1	117.5(5)	O1-Fe1-N2	99.83(7)	C19-N1-Fe1	112.8(2)
C27-N3-Fe1	110.3(5)	C8-N1-Fe1	106.98(13)	C7-N1-Fe1	109.8(2)
O1-Fe1-N2	104.3(2)	C22-N1-Fe1	113.22(14)	O3-Fe1-N3	78.30(11)
O3-Fe1-N2	89.0(2)	C7-N1-Fe1	110.16(14)	O1-Fe1-N2	96.06(13)
N3-Fe1-N2	167.4(2)	O5-Fe1-N2	92.09(67)	O2-Fe1-N2	89.62(11)
O2-Fe1-N1	165.1(2)	N3-Fe1-N2	167.65(7)	O3-Fe1-N2	89.46(12)
O1-Fe1-N1	85.0(2)	O2-Fe1-N1	164.80(7)	N3-Fe1-N2	166.12(13)
O3-Fe1-N1	87.1(2)	O1-Fe1-N1	85.79(6)	C10-N2-Fe1	107.3(3)
N3-Fe1-N1	101.9(3)	O5-Fe1-N1	87.61(7)	C9-N2-Fe1	107.3(2)
C18-N2-Fe1	113.2(5)	N3-Fe1-N1	93.75(7)	C20-N2-Fe1	113.5(2)
N2-Fe1-N1	78.0(2)	N2-Fe1-N1	78.54(7)	C31-N3-Fe1	109.8(2)
C1-O1-Fe1	131.1(5)	C1-O1-Fe1	139.81(14)	O1-Fe1-N1	84.78(11)
C8-N1-Fe1	107.9(5)	C23-N2-Fe1	111.59(14)	O2-Fe1-N1	168.70(10)
C17-N1-Fe1	109.8(6)	C10-N2-Fe1	108.78(12)	O3-Fe1-N1	86.97(11)
C7-N1-Fe1	111.3(5)	C9-N2-Fe1	108.93(14)	N3-Fe1-N1	93.38(10)
C9-N2-Fe1	107.0(5)	C29-N3-Fe1	129.34(17)	N2-Fe1-N1	79.31(11)

Table 3. Selected bond lengths [Å] and angles [deg] for $FeQL^{NEC}$

Molecule 1		**Molecule 2**	
Bond lengths/ Å			
Fe1-O2	1.912(2)	Fe2-O32	1.916(3)
Fe1-O1	1.921(2)	Fe2-O31	1.925(3)
Fe1-O3	1.978(2)	Fe2-O33	1.983(3)
Fe1-N3	2.147(3)	Fe2-N33	2.132(3)
Fe1-N1	2.173(3)	Fe2-N32	2.199(3)
Fe1-N2	2.303(3)	Fe2-N31	2.300(3)
Bond angles/°			
O2-Fe1-O1	91.75(10)	O32-Fe2-O31	92.66(11)
O2-Fe1-O3	169.77(11)	O31-Fe2-O33	167.39(11)
O1-Fe1-O3	94.88(11)	O32-Fe2-O33	95.53(12)
O2-Fe1-N3	92.27(11)	O31-Fe2-N33	90.54(11)
O1-Fe1-N3	101.52(11)	O32-Fe2-N33	101.88(11)
O3-Fe1-N3	78.78(10)	O33-Fe2-N33	78.40(11)
O2-Fe1-N1	101.41(11)	O31-Fe2-N32	103.87(11)
O1-Fe1-N1	87.38(11)	O31-Fe2-N31	85.69(11)
O3-Fe1-N1	86.70(10)	O33-Fe2-N31	88.97(12)
N3-Fe1-N1	163.49(11)	N33-Fe2-N32	163.31(12)
O2-Fe1-N2	85.11(10)	O32-Fe2-N32	86.03(11)
O1-Fe1-N2	166.00(11)	O32-Fe2-N31	164.26(12)
O3-Fe1-N2	90.25(11)	O33-Fe2-N32	86.28(11)
N3-Fe1-N2	92.24(11)	N33-Fe2-N31	93.79(12)
N1-Fe1-N2	79.90(11)	N32-Fe2-N31	79.20(12)
C1-O1-Fe1	133.1(2)	C31-O31-Fe2	133.6(2)
C17-N1-Fe1	113.5(2)	C47-N31-Fe2	111.7(3)
C8-N1-Fe1	107.8(2)	C38-N31-Fe2	107.1(2)
C7-N1-Fe1	108.8(2)	C37-N31-Fe2	111.5(2)
C18-N2-Fe1	110.0(2)	C48-N32-Fe2	111.8(2)
C9-N2-Fe1	107.2(2)	C39-N32-Fe2	107.2(2)
C10-N2-Fe1	112.0(2)	C40-N32-Fe2	108.6(2)
C16-O2-Fe1	133.7(2)	C46-O32-Fe2	134.1(2)

Table 4. λ_{max}/nm (ε/M^{-1} cm^{-1}) LMCT band of complexes $FeQL^{NER}$

$FeQL^{NER}$	**$\varepsilon \times 10^{-5}$ (M^{-1} cm^{-1}) λ_{max} (nm)**		**λ_{max} (nm)**	**$\varepsilon \times 10^{-5}$ (M^{-1} cm^{-1})**
$FeQL^{NEB}$	288	(0.8)	480	(0.3)
$FeQL^{NEC}$	279	(0.7)	477	(0.3)
$FeQL^{NEOB}$	290	(0.6)	556	(0.2)
$FeQL^{NEM}$	310	(1.3)	522	(0.8)

Table 5. Calculated parameters C, μ_{eff} and θ from the fit of the measured data.

$FeQL^{NER}$	**C (emu K/mol)**	**θ (K)**	**μ_{eff} (BM)**
$FeQL^{NEB}$	4.2	-0.93	5.8
$FeQL^{NEC}$	4.1	-0.1	5.7
$FeQL^{NEM}$	3.7	0.0	5.4
$FeQL^{NEOB}$	5.0	1.0	6.3

Table 6. Electrode peak potentials for oxidation and reduction of the complexes $FeQL^{NER}$ measured at ambient temperature in CH_2Cl_2 solutions and referenced vs. the Fc^+/Fc couple.

	E_1^{ox}/V	E_2^{ox}/V	E_1^{red}/V	E_2^{red}/V
$FeQL^{NEB}$	0.59	–	–0.82	–
$FeQL^{NEC}$	0.68	–	–0.79	–
$FeQL^{NEM}$	0.59	–	–0.98	–
$FeQL^{NEOB}$	0.25	0.59	-1.2	-

Figures

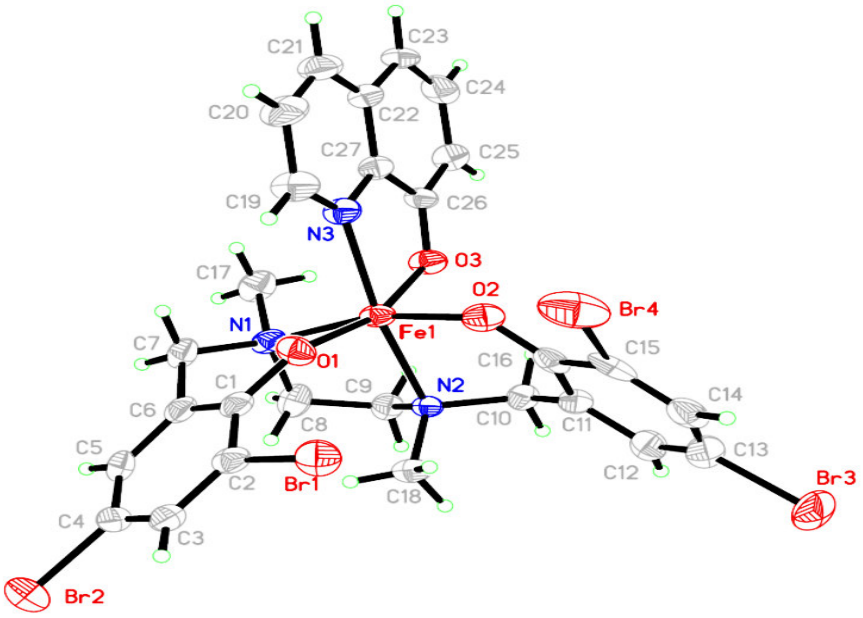

Figure 1. ORTEP diagram and atom labelling scheme for the complex $FeQL^{NEB}$. Ellipsoids plotted at the 30% probability level.

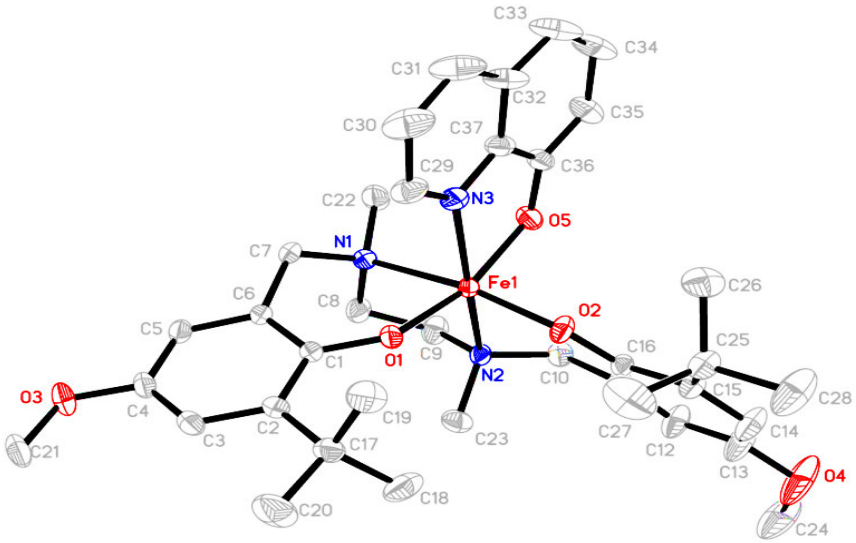

Figure 2. ORTEP diagram and atom labelling scheme for the complex $FeQL^{NEOB}$. Ellipsoids plotted at the 30% probability level. Hydrogen atoms are omitted for clarity.

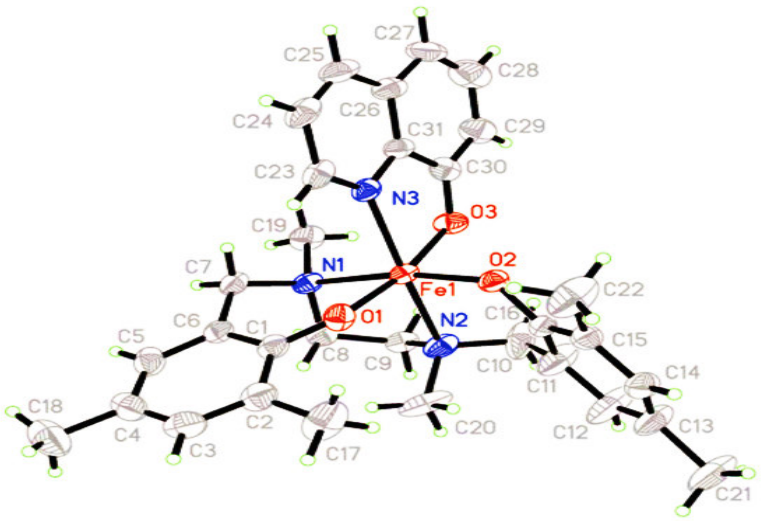

Figure 3. ORTEP diagram and atom labelling scheme for the complex FeQL^{NEM}. Ellipsoids plotted at the 30% probability level.

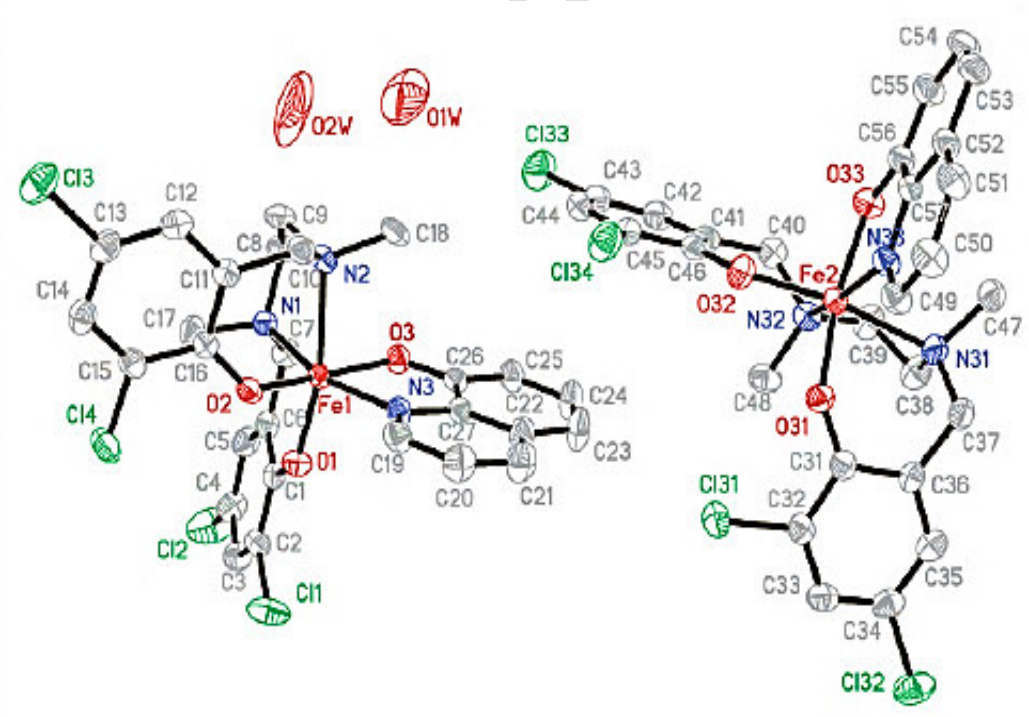

Figure 4. ORTEP diagram and atom labelling scheme for the complex FeQL^{NEC}. Ellipsoids plotted at the 30% probability level. Hydrogen atoms are omitted for clarity.

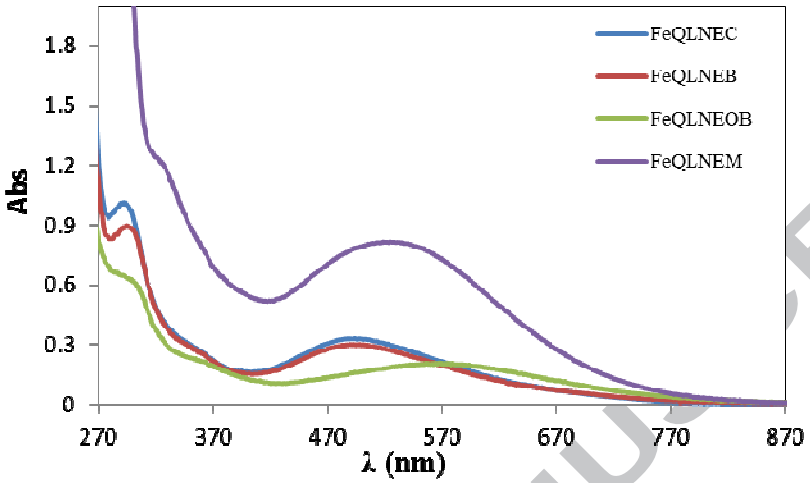

Figure 5. Electronic absorption spectra of $FeQL^{NER}$ in (10 μM) CH_2Cl_2 solution

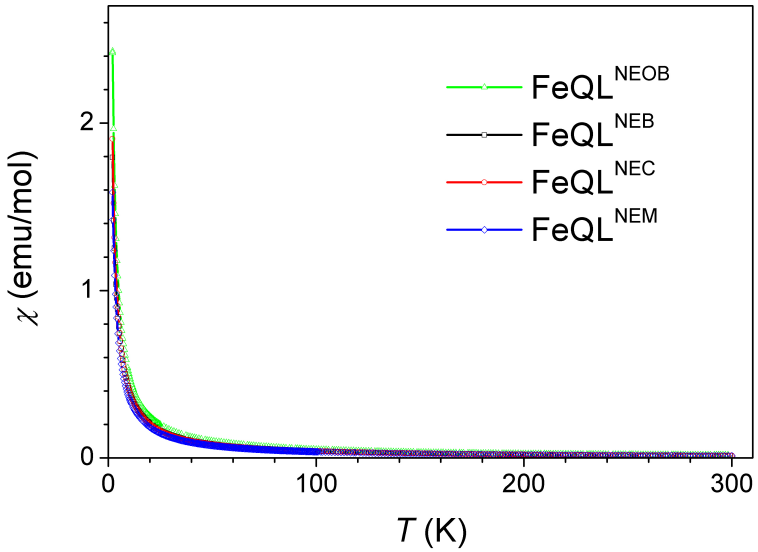

Figure 6. Temperature dependence of the susceptibility$\chi(T)$ of the $FeQL^{NEOB}$, $FeQL^{NEB}$, $FeQL^{NEC}$, and $FeQL^{NEM}$ complexes measured in a magnetic field of H = 1000 Oe

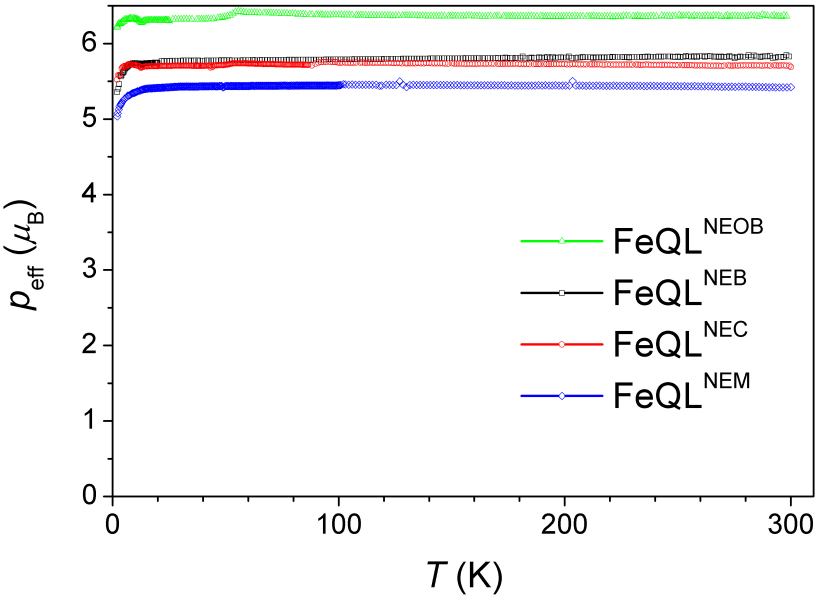

Figure 7. Temperature dependence of the effective magnetic moments for all four samples

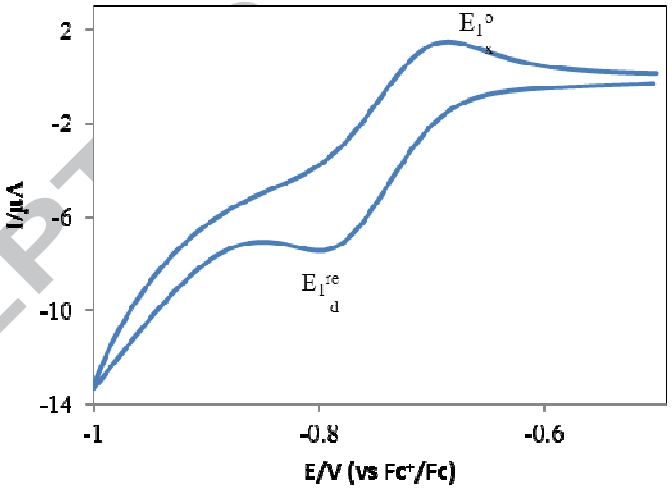

Figure 8. Cyclic voltammogram (reduction process) of the $FeQL^{NEC}$ complex in CH_2Cl_2 at -80°C (sc 100 mV s^{-1})

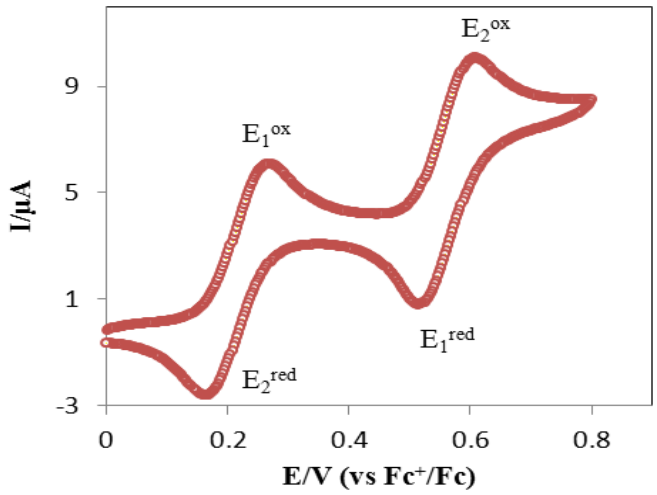

Figure 9. Cyclic voltammogram (oxidation process) of the $FeQL^{NEOB}$ complex in CH_2Cl_2 at -80 °C (sc 100 mV s^{-1})

New Mixed-Ligand 8-Hydroxyquinolinato Iron(III) Complexes of Dimethylethylenediamine-based Aminophenol Ligands

Four new mixed ligand iron(III) complexes of N,N'-dimethylethylenediamine based bis(phenol) di-amine (H_2L^{NER}) and 8-hydroxyquinoline(HQ) ligands have been synthesized and characterized by spectroscopic methods, X-ray diffraction, magnetic susceptibility measurements and cyclic voltammetry techniques.